Article

Analysis and Mitigating Methods for Jamming in the Optical Reconfigurable Intelligent Surfaces-Assisted Dual-Hop FSO Communication Systems

Jingyu Wang [1,2] **, Dingshan Gao** [1,]*** , Juan Li** [2] **, Linhe Huang** [1] **, Haiyang Ding** [2] **and Shaohua Zhou** [2]

[1] Wuhan National Laboratory for Optoelectronics, School of Optoelectronic Science and Engineering, Huazhong University of Science and Technology, Wuhan 430074, China
[2] School of Information and Communication, National University of Defense Technology, Wuhan 430035, China; zhoushaohua17@nudt.edu.cn (S.Z.)
***** Correspondence: dsgao@hust.edu.cn

Abstract: In this paper, we present a study investigating the impact of jamming in a Dual-Hop free-space optical (FSO) communication system assisted by reconfigurable intelligent surfaces (RIS) in the presence of a malicious jammer. We analyze the combined effects of atmospheric turbulence (AT), pointing error (PE), and angle of arrival (AoA) fluctuation of unmanned aerial vehicles (UAVs). Closed-form expressions for the overall average bit error rate (ABER) are derived while considering these impairments. To mitigate the jamming effect, we explore a Single-Input Multiple-Output (SIMO) FSO system and derive the end-to-end Average Bit Error Rate (ABER) under various jamming scenarios. Additionally, we conduct a comprehensive study by examining different placements of the malicious UAV jammer and RIS, drawing insightful conclusions on system performance. The analytically derived expressions are validated through Monte Carlo simulations.

Keywords: ABER; jamming; SIMO; RIS; FSO; UAVs

1. Introduction

With the advancement of society towards full automation and remote management systems, there is a significant demand for network systems capable of handling a large number of transceivers [1]. Primary attributes of fifth-generation and future communication systems consist of robust security protocols, ultra-low latency (as low as 0.1 milliseconds), and remarkably high data transfer capacities (up to 1 Terabit per second) [2,3]. FSO technology is capable of providing very high data transmission rates, high security, and low latency compared to radio frequency (RF) technology, offering advantages in these aspects [4,5]. Furthermore, FSO offers advantages such as unlicensed spectrum usage and low installation costs [3,4]. These features make FSO an optimal technological solution for the imminent advent of fifth-generation and the subsequent sixth generation of wireless communication systems [6]. However, due to the nature of FSO as a line-of-sight (LoS) technology, it is highly susceptible to AT [7], PE [8], and other factors [9], which make long-distance communication challenging [3,10]. Numerous methodologies have been developed to enhance FSO communication [7–9].

In recent times, RIS have emerged as a promising innovation in the research field. Their objective is to mitigate LOS limitations for FSO links through active control over the direction of reflected beams [11,12]. RIS modules are passive components that operate autonomously without the need for a dedicated power source [13]. Since RIS only needs to reflect incident waves in the desired direction, there is no need for analog-to-digital/digital-to-analog converters or power amplifier circuits, thereby avoiding the impact of receiver noise [14,15]. These advantages make RIS a cost-effective, easy-to-deploy, and energy-efficient relay that can be used in wireless RF and FSO communication systems [16,17].

In [12], Najafi et al. investigated the use of intelligent reflecting surfaces to relax the LoS requirement of FSO systems. Naik et al. in [8] implemented an RIS-assisted FSO system in a smart city scenario and studied the impact of signal blockage and Gamma-Gamma (G-G) turbulence on the system performance. In [18], Ndjiongue et al. gave an analysis of RIS-Based Terrestrial-FSO Link Over G-G Turbulence With Distance and Jitter Ratios. In [19], Huang, J. et al. have presented a feasible multi-branch wireless optical communication setup utilizing optical reconfigurable intelligent surfaces. In [18,20], the authors introduced a unified end-to-end Probability Density Function (PDF) expression for a terrestrial FSO RIS system considering the combined impact of G-G atmospheric turbulence, pointing error on the S-IRS/IRS-D links, pointing error ratios, and the placement of the RIS. In summary, RIS integration in FSO communication indeed offers several compelling advantages that directly address the mentioned challenges:

(1) Mitigation of Atmospheric Transmission Losses: By leveraging RIS, we can manipulate the propagation path of signals, thereby reducing losses incurred due to atmospheric transmission [19]. RIS facilitates directing signals towards the intended receiver, effectively minimizing transmission distances and associated losses within the atmosphere [12].

(2) Compensation for Pointing Errors: RIS provides the capability to adjust phase and amplitude during signal propagation, offering compensation for pointing errors. Through the intelligent modulation capabilities of RIS, we can achieve more precise signal alignment, thus enhancing system stability and performance [18,20].

However, FSO systems are mainly vulnerable to malicious jamming signals due to three key factors. (1) In FSO communications, the selection of operational wavelengths is very limited. Some operational wavelengths for FSO transmission include 830 nm, 1300 nm, and 1550 nm [21]. Considering eye safety and lower optical losses, 1550 nm is the most commonly used operational wavelength in many FSO-based applications [21]. Consequently, it is relatively easy for jammer to determine the operational wavelength of dedicated FSO communication links; (2) To mitigate the impact of fading effects such as AT and PE on FSO systems, it is common practice to increase the receiver aperture Field-of-View (FoV) [22]. Enlarging the receiver FOV also makes it feasible to jam optical beams. Many terrestrial applications, such as storage area networks and enterprise connectivity, require aperture averaging and a wide FoV to mitigate the effects of building sway, seismic activity, or physical obstruction, even when the transceiver is stationary [23]. In the satellite communication, a wider FoV is particularly crucial due to the mobility of transceivers and their significant distance from each other [24]; (3) In FSO communication, which belongs to LoS communication, communication antennas are typically installed at the top of buildings along streets or in elevated and easily accessible locations to avoid obstructions [21]. Consequently, malicious jammers may easily identify the locations for jamming.

Researchers have proposed analytical models and methods to mitigate malicious jamming, analyze its impact on the communication performance of FSO systems. In [25] the authors investigated the impact of pulse jamming on FSO systems, focusing primarily on the system's Bit Error Rate (BER) and Outage Probability (OP). The study explored the impact of jamming on the system using different receiver apertures in [25]. In [24], an examination was conducted to analyze the impact of jamming on FSO systems, including both single-input single-output (SISO) setups and multiple-input single-output (MISO) configurations. The study assessed the efficacy of these systems by examining the BER and OP in the presence of negative exponential atmospheric turbulence. In [26], A Buffer-Aided Relaying Approach is employed to mitigate jamming in FSO cooperative networks. In [27], Saxena et al. explore the consequences of jamming instigated by a malicious UAV on the performance of an FSO communication system. They utilize a trustworthy UAV as a relay and incorporate an intelligent reflecting surface to improve signal coverage.

However, in all of these works, research on FSO jamming and mitigation techniques is primarily focused on single-hop systems. Furthermore, while literature has conducted jamming mitigation analysis using MISO for single-hop systems, SIMO is relatively easier

to implement compared to MISO. Therefore, this prompts us to delve into examining the ABER of dual-hop FSO systems supported by RIS in the presence of jamming. Additionally, we aim to evaluate the improvement of ABER under different jamming scenarios utilizing SIMO technology. In summary, the key contributions of this study can be outlined as follows:

- The closed-form expression of the PDF of the legitimate channel in the RIS-assisted dual-hop FSO system is derived. Additionally, The PDF of the UAV jamming receiver and the RIS channel is derived. Novel closed-form expressions for the end-to-end ABER in both jamming scenarios have been derived based on the obtained link statistics. These expressions are derived considering the impact of non-Gaussian additive noise, which varies depending on the jammer's location.
- The closed-form PDF of the legitimate channel in a $1 \times N$ SIMO-FSO system and the channels under various jamming scenarios were derived using Mellin transforms to mitigate the impact of jamming. Analytical expressions for the end-to-end ABER in the two jamming scenarios were subsequently provided.
- A comprehensive system ABER analysis is conducted in terms of atmospheric turbulence strength, N (the number of receiving apertures), the probability of jamming and different RIS positions. Moreover, some useful insights are obtained.

The rest of the paper is organized as follows. The FSO system, along with the jammer and optical channel models, is introduced in Section 2. In Section 3, The closed-form expressions for ABER in the SISO System are derived. In Section 4, ABER analysis is carried for a generalized N receiving apertures with a jammer. The numerical results and discussion are presented in Section 5, and we conclude this paper in Section 6.

2. System and Channel Model

2.1. System Model

RIS-assisted FSO communication is shown in Figure 1. There is no direct LoS between the source (S) and the destination (D) due to the obstruction caused by some building and obstacles. The source is equipped with a LD which transmits symbols employing intensity modulation and direct detection (IM/DD) and on-off shift keying (OOK) modulation schemes. A malicious jammer, which UAVs are equipped with, is randomly present, attempting to disrupt the legitimate transmission link by opportunistically sending an optical signal. Thus, at any given instant, the jammer can jam either the received signal at the RIS or the received signal at the destination. Therefore, we consider two jamming scenarios: Scenario 1 involves a malicious jammer causing jamming at the destination, as depicted in Figure 1a, and Scenario 2 involves a malicious jammer causing jamming at the RIS, as depicted in Figure 1b.
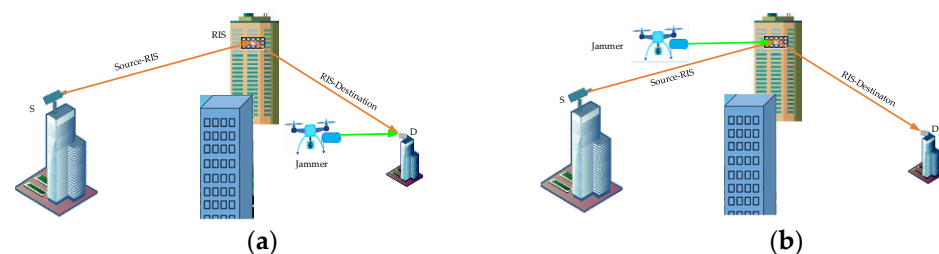

(**a**)　　　　　　　　　　　　　　　　　(**b**)

Figure 1. The proposed system model. (**a**) Jamming at the destination, (**b**) Jamming at RIS.

2.1.1. System Model for Scenario 1

The signal from S is transmitted to D through the RIS consisting of N reflecting elements. Each component of the RIS receives the incident light and adjusts the phase and amplitude under program control, and then transmits it to the receiver. It is assumed that the signal transmitted through the RIS is fully radiated and undergoes full phase compensation. The received signal is given as

$$y_1 = R\sqrt{P_s}h_i s + R\sqrt{N_J}h_J \Lambda s_J + n \tag{1}$$

where R is related to the responsivity of the photodetector, whose value is considered as 1; s represents the modulated information symbol; $h_i = h_p \partial e^{j\Psi_p} h_q$, h_p, h_q and h_J are the S-RIS, RIS-D and jammer channel fading coefficient, respectively; $\partial e^{j\Psi_p}$ characterizes the IRS element at a position P, with ∂ representing the amplitude reflection coefficient and Ψ_p denoting the induced phase; s_J is the injected jamming signal, whose value is considered as unity; P_s represents the peak transmit energy of the legitimate transmitter; n is the additive white Gaussian noise (AWGN) with zero mean and variance N_0; Λ represents the state of jamming, modeled using a Bernoulli distributed random variable, Thus, the probability distribution of Λ is given by [24]

$$\begin{cases} P(\Lambda = 1) = \rho \\ P(\Lambda = 0) = 1 - \rho \end{cases} \tag{2}$$

where $P(\Lambda = 1)$ represents the probability of the occurrence of a jamming event; $P(\Lambda = 0)$ represents the probability of the jamming event being idle. we define P_J as the average power of jamming. When the jamming event is in an active state and starts to jam legitimate information, the energy it emits is denoted as $N_J = P_J/\rho$.

The signal-to-jamming-and-noise ratio (SJNR) can be obtained from (1) when the jamming is active.

$$\gamma_1 = \frac{(h_i)^2 P_s}{N_J h_J^2 + N_0} \tag{3}$$

When the jamming is idle, the signal-to-noise ratio (SNR) can be calculated as follows:

$$\gamma_2 = \frac{(h_i)^2 P_s}{N_0} = \overline{\gamma}_D (h_i)^2 \tag{4}$$

where $\overline{\gamma}_D = \frac{P_s}{N_0}$ represents the average signal-to-noise ratio (SNR).

2.1.2. System Model for Scenario 2

As shown in Figure 1b, the RIS is jammed by the UAV. Assuming that the jammer can effectively align to the RIS unit of the legitimate signal. Thus, the received signal at the destination is denoted as

$$y_2 = R\sqrt{P_s}h_i s + R\sqrt{N_J}g_J \Lambda s_J + n \tag{5}$$

where $g_J = h_J \partial e^{j\Psi_p} h_q$.

From (5), it can be derived that the SJNR is obtained when the jamming is active.

$$\gamma_3 = \frac{(h_i)^2 P_s}{(g_J)^2 N_J + N_0} \tag{6}$$

When the jamming is idle, the expression of SNR follows (4).

2.2. Channel Model

FSO communication links are affected by three main sources of signal attenuation: path loss, PE, and AT. These sources of attenuation affect the transmitted optical signal in various ways. The PDF of the channel attenuation factor h_x is as [27]

$$f_{h_x}(h_x) = \frac{\alpha_x \beta_x \xi_x^2}{A_{0_x} \Gamma(\alpha_x)\Gamma(\beta_x)} G_{1,3}^{3,0}\left(\frac{\alpha_x \beta_x h_x}{A_{0_x}} \middle| \begin{matrix} \xi_x^2 \\ \xi_x^2 - 1, \alpha_x - 1, \beta_x - 1 \end{matrix}\right), x \in \{p, q\} \tag{7}$$

Since the jamming event is caused by UAV, the PDF of the channel attenuation factor h_J, considering the fluctuations of AT, PE, and AoA, is as [27]

$$f_{h_J}(h_J) = \exp\left(-\frac{\varphi_{AoA}^2}{2\sigma_{AoA}^2}\right)\delta(h_J) + \left[1 - \exp\left(-\frac{\varphi_{AoA}^2}{2\sigma_{AoA}^2}\right)\right]$$
$$\times \frac{\alpha_J\beta_J\xi_J^2}{A_{0_J}\Gamma(\alpha_J)\Gamma(\beta_J)}G_{1,3}^{3,0}\left(\frac{\alpha_J\beta_Jh_J}{A_{0_J}}\left|\begin{array}{c}\xi_J^2\\\xi_J^2-1,\alpha_J-1,\beta_J-1\end{array}\right.\right)$$

(8)

Here φ_{AoA} is AoA [27], σ_{AoA} is the standard variation of UAV's orientation [28]; α_x, β_x ($x \in \{p, q, J\}$) is the parameters for G-G turbulence for *x*th link, i.e., they attain the values $\{4, 1.9\}$ and $\{4, 1.4\}$ for moderate and strong AT regimes, respectively [28]. ξ_x characterizes the PE faced by legitimate or jammer signal: higher the value of ξ_x, lower the PE [24,27]. $G_{p,q}^{m,n}(\cdot|)$ is the Meijer-G function [29]. $A_{0_x}(x \in \{p, q, J\})$ is the fraction of collected power at the center of beam footprint [27].

According to [30], it is known that $h_i = h_p\partial e^{j\Psi_p}h_q$. Thus, we can obtain

$$f_{h_i}(h_i) = \int_0^\infty f_{h_p}(h_p)f_{h_q}\left(\frac{h_i}{h_p}\right)\frac{1}{h_p}dh_p$$

(9)

By substituting (7) into (9) and integrating using 07.34.16.0002.01 [29] and 07.34.16.0002.01 [29], we obtain

$$f_{h_i}(h_i) = \frac{\alpha_p\beta_p\xi_p^2}{A_{0_p}\Gamma(\alpha_p)\Gamma(\beta_p)}\frac{\alpha_q\beta_q\xi_q^2}{A_{0_q}\Gamma(\alpha_q)\Gamma(\beta_q)}$$
$$\times G_{2,6}^{6,0}\left(\frac{\alpha_p\beta_p\alpha_q\beta_qh_i}{A_{0_p}A_{0_q}}\left|\begin{array}{c}\xi_p^2,\xi_q^2\\\xi_p^2-1,\alpha_p-1,\beta_p-1,\xi_q^2-1,\alpha_q-1,\beta_q-1\end{array}\right.\right)$$

(10)

Since $g_J = h_J\partial e^{j\Psi_p}h_q$, we can obtain

$$f_{g_J}(g_J) = \int_0^\infty f_{h_q}(h_q)f_{h_J}\left(\frac{g_J}{h_q}\right)\frac{1}{h_q}dh_q = I_1 + I_2$$

(11)

By substituting (7) and (8) into (11), integrating using 07.34.16.0002.01 [29], we obtain

$$I_1 = \exp\left(-\frac{\varphi_{AoA}^2}{2\sigma_{AoA}^2}\right)\delta(g_J)$$

(12)

$$I_2 = \frac{\alpha_q\beta_q\xi_q^2}{A_{0_q}\Gamma(\alpha_q)\Gamma(\beta_q)}\left[1 - \exp\left(-\frac{\varphi_{AoA}^2}{2\sigma_{AoA}^2}\right)\right]\frac{\alpha_J\beta_J\xi_J^2}{A_{0_J}\Gamma(\alpha_J)\Gamma(\beta_J)}$$
$$\times G_{2,6}^{6,0}\left(\frac{\alpha_J\beta_J\alpha_q\beta_qg_J}{A_{0_J}A_{0_q}}\left|\begin{array}{c}\xi_J^2,\xi_q^2\\\xi_J^2-1,\alpha_J-1,\beta_J-1,\xi_q^2-1,\alpha_q-1,\beta_q-1\end{array}\right.\right)$$

(13)

3. Analysis of BER for SISO System

3.1. Scenario 1

In this section, the BER performance is evaluated for the SISO FSO system under the presence of jamming or AWGN.

3.1.1. BER during Jamming Active

Let us define a random variable, $T \triangleq \sqrt{N_J}h_J = \sqrt{P_j/\rho}h_J$. Using (8), the PDF of T is given as

$$f_T(T) = \frac{1}{\sqrt{p_J/\rho}} \exp\left(-\frac{\varphi_{AoA}^2}{2\sigma_{AoA}^2}\right) \delta\left(\frac{T}{\sqrt{p_J/\rho}}\right) + \frac{1}{\sqrt{p_J/\rho}} \left[1 - \exp\left(-\frac{\varphi_{AoA}^2}{2\sigma_{AoA}^2}\right)\right]$$
$$\times \frac{\alpha_J \beta_J \xi_J^2}{A_{0_J} \Gamma(\alpha_J) \Gamma(\beta_J)} G_{1,3}^{3,0}\left(\frac{\alpha_J \beta_J T}{A_{0_J}\sqrt{p_J/\rho}} \left| \begin{array}{c} \xi_J^2 \\ \xi_J^2 - 1, \alpha_J - 1, \beta_J - 1 \end{array}\right.\right) \quad (14)$$

When jamming is present, the energy of the jamming significantly outweighs that of Gaussian white noise, which allows us to disregard the Gaussian white noise. Therefore, we can derive that $T = y_1 - \sqrt{P_s}h_i s$. By using (14), we can further deduce that

$$f_{y_1}(y_1) = \frac{1}{\sqrt{p_J/\rho}} \exp\left(-\frac{\varphi_{AoA}^2}{2\sigma_{AoA}^2}\right) \delta\left(\frac{y_1 - \sqrt{P_s}h_i s}{\sqrt{p_J/\rho}}\right) + \frac{1}{\sqrt{p_J/\rho}} \left[1 - \exp\left(-\frac{\varphi_{AoA}^2}{2\sigma_{AoA}^2}\right)\right]$$
$$\times \frac{\alpha_J \beta_J \xi_J^2}{A_{0_J} \Gamma(\alpha_J) \Gamma(\beta_J)} G_{1,3}^{3,0}\left(\frac{\alpha_J \beta_J (y_1 - \sqrt{P_s}h_i s)}{A_{0_J}\sqrt{p_J/\rho}} \left| \begin{array}{c} \xi_J^2 \\ \xi_J^2 - 1, \alpha_J - 1, \beta_J - 1 \end{array}\right.\right) \quad (15)$$

(15) can be expanded based on the value of the symbol s.

$$f_{y_1}(y_1) = \begin{cases} \frac{1}{\sqrt{p_J/\rho}} \exp\left(-\frac{\varphi_{AoA}^2}{2\sigma_{AoA}^2}\right) \delta\left(\frac{y_1}{\sqrt{p_J/\rho}}\right) + \frac{1}{\sqrt{p_J/\rho}} \left[1 - \exp\left(-\frac{\varphi_{AoA}^2}{2\sigma_{AoA}^2}\right)\right] \\ \times \frac{\alpha_J \beta_J \xi_J^2}{A_{0_J} \Gamma(\alpha_J) \Gamma(\beta_J)} G_{1,3}^{3,0}\left(\frac{\alpha_J \beta_J (y_1)}{A_{0_J}\sqrt{p_J/\rho}} \left| \begin{array}{c} \xi_J^2 \\ \xi_J^2 - 1, \alpha_J - 1, \beta_J - 1 \end{array}\right.\right), \quad \text{for } s = 0 \\[4mm] \frac{1}{\sqrt{p_J/\rho}} \exp\left(-\frac{\varphi_{AoA}^2}{2\sigma_{AoA}^2}\right) \delta\left(\frac{y_1 - \sqrt{P_s}h_i}{\sqrt{p_J/\rho}}\right) + \frac{1}{\sqrt{p_J/\rho}} \left[1 - \exp\left(-\frac{\varphi_{AoA}^2}{2\sigma_{AoA}^2}\right)\right] \\ \times \frac{\alpha_J \beta_J \xi_J^2}{A_{0_J} \Gamma(\alpha_J) \Gamma(\beta_J)} G_{1,3}^{3,0}\left(\frac{\alpha_J \beta_J (y_1 - \sqrt{P_s}h_i)}{A_{0_J}\sqrt{p_J/\rho}} \left| \begin{array}{c} \xi_J^2 \\ \xi_J^2 - 1, \alpha_J - 1, \beta_J - 1 \end{array}\right.\right), \quad \text{for } s = 1 \end{cases} \quad (16)$$

ABER can be expressed based on the occurrence of jamming states.

$$P_{e1} = P(\Lambda = 1)[P(x = 1)P(\nu|x = 1) + P(x = 0)P(\nu|x = 0)] + P(\Lambda = 0)P_{ei} \quad (17)$$

where P_{ei} represents BER during jamming idle states and ν denotes the occurrence of a bit error event. Here, we assume $P(x = 1) = P(x = 0) = 0.5$, indicating that the symbols '1' and '0' are transmitted with equal probabilities.

When jamming is active and the jamming noise significantly exceeds the additive white Gaussian noise, the additive white Gaussian noise can be disregarded when calculating BER. As a result, the expression for calculating the BER under jamming active, derived from (17), is as follows

$$P_{e1a} = \rho\left[0.5 \int_{th}^{\infty} f_y(y|s = 0)dy + 0.5 \int_0^{th} f_y(y|s = 1)dy\right] \quad (18)$$

According to [25], $th = \sqrt{P_s}h_i$. Substituting (19) into (21) and integrating using 07.34.21.0084.01 and 07.34.21.0085.01 is as

$$P_{e1a}(h_i) = \frac{\rho}{2}\left[1 - \exp\left(-\frac{\varphi_{AoA}^2}{2\sigma_{AoA}^2}\right)\right] \frac{\alpha_J \beta_J \xi_J^2 \sqrt{\rho \overline{\gamma}_{JD}} h_i}{A_{0_J} \Gamma(\alpha_J) \Gamma(\beta_J)}$$
$$\times G_{2,4}^{4,0}\left(\frac{\alpha_J \beta_J h_i \sqrt{\rho \overline{\gamma}_{JD}}}{A_{0_J}} \left| \begin{array}{c} \xi_J^2, 0 \\ -1, \xi_J^2 - 1, \alpha_J - 1, \beta_J - 1 \end{array}\right.\right) \quad (19)$$

According to [25], in the presence of jamming, we can derive the expression for ABER from (19) as follows

$$P_{e1a}\left(\overline{\gamma}_{JD}\right) = \int_0^{\infty} P_{e1a}(h_i) f_{h_i}(h_i) dh_i \quad (20)$$

By substituting (10) and (19) into (20) and integrating using 07.34.21.0011.01 [29], we can obtain

$$P_{e1a}\left(\overline{\gamma}_{JD}\right) = \frac{\xi_p^2}{\Gamma(\alpha_p)\Gamma(\beta_p)} \frac{\xi_q^2}{\Gamma(\alpha_q)\Gamma(\beta_q)} \frac{\rho}{2} \left[1 - \exp\left(-\frac{\varphi_{AoA}^2}{2\sigma_{AoA}^2}\right)\right] \frac{\alpha_J \beta_J \xi_J^2 \sqrt{\rho \overline{\gamma}_{JD}}}{A_{0_J}\Gamma(\alpha_J)\Gamma(\beta_J)}$$
$$\times \frac{A_{0_p} A_{0_q}}{\alpha_p \beta_p \alpha_q \beta_q} G_{8,6}^{4,6}\left(\frac{\alpha_J \beta_J A_{0_p} A_{0_q} \sqrt{\rho \overline{\gamma}_{JD}}}{\alpha_p \beta_p \alpha_q \beta_q A_{0_J}}\middle|\begin{array}{l} -\xi_p^2, -\alpha_p, -\beta_p, -\xi_q^2, -\alpha_q, -\beta_q, \xi_J^2, 0 \\ -1, \xi_J^2 - 1, \alpha_J - 1, \beta_J - 1, -1 - \xi_p^2, -1 - \xi_q^2 \end{array}\right) \tag{21}$$

where $\overline{\gamma}_{JD} = \frac{P_s}{P_J}$ is average signal jamming ratio (SJR).

3.1.2. BER during Jamming Idle

In the absence of jamming, when the system is only subjected to AWGN, we can derive the following expression from (4) and (10)

$$f_{\gamma_2}(\gamma_2) = \frac{\alpha_p \beta_p \xi_p^2}{2\sqrt{\gamma_2 \overline{\gamma}_D} A_{0_p}\Gamma(\alpha_p)\Gamma(\beta_p)} \frac{\alpha_q \beta_q \xi_q^2}{A_{0_q}\Gamma(\alpha_q)\Gamma(\beta_q)}$$
$$\times G_{2,6}^{6,0}\left(\frac{\alpha_p \beta_p \alpha_q \beta_q}{A_{0_p} A_{0_q}}\sqrt{\frac{\gamma_2}{\overline{\gamma}_D}}\middle|\begin{array}{l} \xi_q^2, \xi_p^2 \\ \xi_p^2 - 1, \alpha_p - 1, \beta_p - 1, \xi_q^2 - 1, \alpha_q - 1, \beta_q - 1 \end{array}\right) \tag{22}$$

According to [31], ABER in a system affected by AWGN is given by

$$P_{e1i}(\overline{\gamma}_D) = 0.5 \int_0^\infty erfc\left(\frac{\sqrt{\gamma_2}}{2\sqrt{2}}\right) f_{\gamma_2}(\gamma_2) d\gamma_2 \tag{23}$$

where *erfc* can be expressed by Meijer-G function [32].

$$erfc(\sqrt{y}) = \frac{1}{\sqrt{\pi}} G_{1,2}^{2,0}\left[y\middle|\begin{array}{l} 1 \\ 0, 1/2 \end{array}\right] \tag{24}$$

By substituting (22) and (24) into (23) and integrating using 07.34.21.0013.01, the ABER under jamming idle can be obtained as follows

$$P_{e1i}(\overline{\gamma}_D) = \frac{1}{\sqrt{\pi}} \frac{2^{(\alpha_p + \beta_p + \alpha_q + \beta_q - 7)}}{(\pi)^2} \frac{\xi_p^2}{\Gamma(\alpha_p)\Gamma(\beta_p)} \frac{\xi_q^2}{\Gamma(\alpha_q)\Gamma(\beta_q)}$$
$$\times G_{13,6}^{2,12}\left(32\overline{\gamma}_D\left(\frac{A_{0_p} A_{0_q}}{\alpha_p \beta_p \alpha_q \beta_q}\right)^2\middle|\begin{array}{l} \Xi_1, \Xi_2, \Xi_3, 1 \\ 0, \frac{1}{2}, \frac{1 - \xi_p^2}{2}, \frac{2 - \xi_p^2}{2}, \frac{1 - \xi_q^2}{2}, \frac{2 - \xi_q^2}{2} \end{array}\right) \tag{25}$$

where $\Xi_1 = \frac{1 - \xi_p^2}{2}, \frac{2 - \xi_p^2}{2}, \frac{1 - \alpha_p}{2}, \frac{2 - \alpha_p}{2}$, $\Xi_2 = \frac{1 - \beta_p}{2}, \frac{2 - \beta_p}{2}, \frac{1 - \xi_q^2}{2}, \frac{2 - \xi_q^2}{2}$, and $\Xi_3 = \frac{1 - \alpha_q}{2}, \frac{2 - \alpha_q}{2}, \frac{1 - \beta_q}{2}, \frac{2 - \beta_q}{2}$.

The overall ABER of the proposed system for scenario 1 can be expressed as follows

$$\overline{P}_{e1a} = \rho P_{e1a}\left(\overline{\gamma}_{JD}\right) + (1 - \rho)P_{e1i}(\overline{\gamma}_D) \tag{26}$$

3.2. Scenario 2

Similar to scenario 1, ABER under jamming for scenario 2 can be obtained as

$$P_{e2a}\left(\overline{\gamma}_{JD}\right) = \frac{A_{0_p}\xi_p^2}{\alpha_p \beta_p \Gamma(\alpha_p)\Gamma(\beta_p)} \frac{\xi_q^2}{\Gamma(\alpha_q)\Gamma(\beta_q)} \frac{\rho \sqrt{\rho \overline{\gamma}_{JD}}\xi_q^2}{2\Gamma(\alpha_q)\Gamma(\beta_q)}$$
$$\times \left[1 - \exp\left(-\frac{\varphi_{AoA}^2}{2\sigma_{AoA}^2}\right)\right] \frac{\alpha_J \beta_J \xi_J^2}{A_{0_J}\Gamma(\alpha_J)\Gamma(\beta_J)}$$
$$\times G_{9,9}^{7,6}\left(\frac{\alpha_J \beta_J A_{0_p} \sqrt{\rho \overline{\gamma}_{JD}}}{A_{0_J}\alpha_p \beta_p}\middle|\begin{array}{l} \Theta_1, \Theta_2 \\ \Theta_3, \Theta_4 \end{array}\right) \tag{27}$$

where $\Theta_1 = -\xi_p^2, -\alpha_p, -\beta_p, -\xi_q^2$, $\Theta_2 = -\alpha_q, -\beta_q, \xi_J^2, \xi_q^2, 0$, $\Theta_3 = -1, \xi_q^2 - 1, \alpha_q - 1, \beta_q - 1, \xi_J^2 - 1$, and $\Theta_4 = \alpha_J - 1, \beta_J - 1, -1 - \xi_p^2, -1 - \xi_q^2$.

When the jamming is idle, the system and channel models in scenario 1 and scenario 2 are identical. Therefore, the BER between scenario 2 and scenario 1 is the same when the jamming is idle. Consequently, we can obtain the ABER in scenario 2 as follows

$$\overline{P}_{e2a} = \rho P_{e2a}\left(\overline{\gamma}_{JD}\right) + (1-\rho)P_{e1i}(\overline{\gamma}_D) \tag{28}$$

4. Methods for Mitigating Jamming

In this section, the study extends to the evaluation of error performance in the presence of a jammer for a general SIMO FSO communication system. SIMO technology can mitigate jamming factors such as signal attenuation and atmospheric turbulence in the transmission link, thereby enhancing the reliability of communication systems. Even if one receiver encounters jamming, other receivers can still receive the optical signal. They can then perform merging and processing in the signal processing unit to recover the original data. Now, we analyze the impact of jamming on the communication performance of SIMO FSO systems.

4.1. Scenario 1

When the jammer is located at the destination, we can obtain the value of the n-th receiving aperture after photoelectric conversion as follows:

$$y_n = Ra_n h_{in}\sqrt{P_s}s + R\sqrt{N_J}h_J\Lambda s_J + n_n \tag{29}$$

where h_{in} represents the attenuation coefficient of the n-th channel; a_n represents the weighted value of the n-th channel; For the purpose of simplifying calculations, we assume that $a_n = \frac{1}{N}$; n_n is the AWGN with zero mean and variance N_0; $\frac{1}{N}$ represents the jamming from N receiving apertures at the receiver, which follows a uniform distribution. Therefore, the probability of jamming for any one of them is $\frac{1}{N}$.

The receiver combines the received electrical signals by using the equal gain combining (EGC) [33] as follows:

$$y_D = \sum_{n=1}^{N} y_n = R\sqrt{P_s}s\sum_{n=1}^{N} a_n h_{in} + R\sqrt{N_J}h_J\Lambda s_J + \sum_{n=1}^{N} n_n \tag{30}$$

From (30), we can obtain the received SJR as follows

$$\gamma_{SJR-D} = \frac{P_s\left(\sum\limits_{n=1}^{N} a_n h_{in}\right)^2}{N_J(h_J)^2} = \frac{\rho\overline{\gamma}_{JD}\left(\sum\limits_{n=1}^{N} a_n h_{in}\right)^2}{(h_J)^2} \tag{31}$$

We can also obtain from (30) the received SNR as follows

$$\gamma_{SNR} = \frac{P_s\left(\sum\limits_{n=1}^{N} a_n h_{in}\right)^2}{NN_0} = \frac{\overline{\gamma}_D\left(\sum\limits_{n=1}^{N} a_n h_{in}\right)^2}{N} \tag{32}$$

4.2. Scenario 2

When the jammer jams the IRS, we assume that the jamming optical path can effectively align with the legitimate optical path unit of the IRS. As a result, we can obtain the received signal for the n-th path as follows

$$y_{n-IRS} = Ra_n h_{in}\sqrt{P_s}s + R\sqrt{N_J}b_n h_{Jn}\Lambda s_J + n_n \tag{33}$$

where b_n represents the weighting value of the nth interfering branch, similarly, we assume $b_n = \frac{1}{N}$.

The receiver combines the received electrical signals by using the EGC as follows

$$y_{I-D} = \sum_{n=1}^{N} y_{n-IRS} = R\sqrt{P_s}s\sum_{n=1}^{N} a_n h_{in} + R\sqrt{N_J}\sum_{n=1}^{N} b_n g_{Jn}\Lambda s_J + \sum_{n=1}^{N} n_n \tag{34}$$

From (34), we can calculate the SJR at the receiver as

$$\gamma_{SJR-R} = \frac{P_s\left(\sum\limits_{n=1}^{N} a_n h_{in}\right)^2}{N_J\left(\sum\limits_{n=1}^{N} b_n h_{Jn}\right)^2} = \frac{\rho\overline{\gamma}_{JD}\left(\sum\limits_{n=1}^{N} a_n h_{in}\right)^2}{\left(\sum\limits_{n=1}^{N} b_n h_{Jn}\right)^2} \tag{35}$$

4.3. ABER Calculation

4.3.1. Analysis of the ABER for SIMO in Scenario 1

The PDF of the received signal can be derived from Equations (8) and (30) as follows

$$f_{y_D}(y_D) = \begin{cases} \dfrac{1}{\sqrt{p_J/\rho}}\exp\left(-\dfrac{\varphi_{AoA}^2}{2\sigma_{AoA}^2}\right)\delta\left(\dfrac{y_D}{\sqrt{p_J/\rho}}\right) \\[2ex] \quad + \dfrac{1}{\sqrt{p_J/\rho}}\left[1-\exp\left(-\dfrac{\varphi_{AoA}^2}{2\sigma_{AoA}^2}\right)\right]\dfrac{\alpha_J\beta_J\xi_J^2}{A_{0_J}\Gamma(\alpha_J)\Gamma(\beta_J)} \\[2ex] \quad \times G_{1,3}^{3,0}\left(\dfrac{\alpha_J\beta_J y_D}{A_{0_J}\sqrt{p_J/\rho}}\,\middle|\,\begin{matrix}\xi_J^2 \\ \xi_J^2-1,\alpha_J-1,\beta_J-1\end{matrix}\right), & \text{for } s=0 \\[4ex] \dfrac{1}{\sqrt{p_J/\rho}}\exp\left(-\dfrac{\varphi_{AoA}^2}{2\sigma_{AoA}^2}\right)\delta\left(\dfrac{y_D-\sqrt{P_s}s\sum\limits_{n=1}^{N}a_n h_{in}}{\sqrt{p_J/\rho}}\right) \\[2ex] \quad + \dfrac{1}{\sqrt{p_J/\rho}}\left[1-\exp\left(-\dfrac{\varphi_{AoA}^2}{2\sigma_{AoA}^2}\right)\right]\dfrac{\alpha_J\beta_J\xi_J^2}{A_{0_J}\Gamma(\alpha_J)\Gamma(\beta_J)} \\[2ex] \quad \times G_{1,3}^{3,0}\left(\dfrac{\alpha_J\beta_J\left(y_D-\sqrt{P_s}s\sum\limits_{n=1}^{N}a_n h_{in}\right)}{A_{0_J}\sqrt{p_J/\rho}}\,\middle|\,\begin{matrix}\xi_J^2 \\ \xi_J^2-1,\alpha_J-1,\beta_J-1\end{matrix}\right), & \text{for } s=1 \end{cases} \tag{36}$$

Let $h_{sum} = \sum\limits_{n=1}^{N} a_n h_{in}$, then by substituting (18) and (36), we obtain

$$P_{e1a}(h_i) = \frac{\rho}{2}\left[1-\exp\left(-\frac{\varphi_{AoA}^2}{2\sigma_{AoA}^2}\right)\right]\frac{\alpha_J\beta_J\xi_J^2\sqrt{\rho\overline{\gamma}_J}h_{sum}}{A_{0_J}\Gamma(\alpha_J)\Gamma(\beta_J)}$$
$$\times G_{2,4}^{4,0}\left(\frac{\alpha_J\beta_J\sqrt{\rho\overline{\gamma}_J}h_{sum}}{A_{0_J}}\,\middle|\,\begin{matrix}\xi_J^2,0 \\ -1,\xi_J^2-1,\alpha_J-1,\beta_J-1\end{matrix}\right) \tag{37}$$

Then, we apply the Mellin transform to (43) using 07.34.22.0004.01 [29], which results in

$$\varphi_{h_{in}}(z) = \frac{\alpha_q\beta_q\xi_q^2}{A_{0_q}\Gamma(\alpha_q)\Gamma(\beta_q)}\left[1-\exp\left(-\frac{\varphi_{AoA}^2}{2\sigma_{AoA}^2}\right)\right]\frac{\alpha_J\beta_J\xi_J^2}{A_{0_J}\Gamma(\alpha_J)\Gamma(\beta_J)}\left(\frac{\alpha_J\beta_J\alpha_q\beta_q}{A_{0_J}A_{0_q}}\right)^{-z}$$
$$\times \frac{\Gamma(\xi_J^2-1+z)\Gamma(\alpha_J-1+z)\Gamma(\beta_J-1+z)\Gamma(\xi_q^2-1+z)\Gamma(\alpha_q-1+z)\Gamma(\beta_q-1+z)}{\Gamma(\xi_q^2+z)\Gamma(\xi_J^2+z)} \tag{38}$$

Considering the independent channels, the Mellin transform of h_{sum} can be expressed as

$$\varphi_{h_{sum}}(z) = \prod_{n=1}^{N}\varphi_{h_{in}}(z) = \left(\varphi_{h_{in}}(z)\right)^N \tag{39}$$

By substituting (38) into (39) and performing the Mellin inverse transform, the PDF of h_{sum} can be obtained as follows

$$f_{h_{sum}}(x) = \left(\frac{\alpha_p \beta_p \xi_p^2}{A_{0_p} \Gamma(\alpha_p)\Gamma(\beta_p)} \frac{\alpha_q \beta_q \xi_q^2}{A_{0_q} \Gamma(\alpha_q)\Gamma(\beta_q)} \right)^N$$
$$\times G_{2N,6N}^{6N,0} \left(\left(\frac{\alpha_p \beta_p \alpha_q \beta_q}{A_{0_p} A_{0_q}} \right)^N \times \middle| \begin{array}{c} \mathbf{S}_1 \\ \mathbf{S}_2, \mathbf{S}_3, \mathbf{S}_4 \end{array} \right) \tag{40}$$

where $\mathbf{S}_1 = \overbrace{\xi_p^2, \cdots, \xi_p^2}^{N}, \overbrace{\xi_q^2, \cdots, \xi_q^2}^{N}$, $\mathbf{S}_2 = \underbrace{\xi_p^2 - 1, \cdots, \xi_p^2 - 1}_{N}, \underbrace{\alpha_p - 1, \cdots, \alpha_p - 1}_{N}$,

$\mathbf{S}_3 = \underbrace{\beta_p - 1, \cdots, \beta_p - 1}_{N}, \underbrace{\xi_q^2 - 1, \cdots, \xi_q^2 - 1}_{N}$, and $\mathbf{S}_4 = \underbrace{\alpha_q - 1, \cdots, \alpha_q - 1}_{N}, \underbrace{\beta_q - 1, \cdots, \beta_q - 1}_{N}$.

Now, using (37), (40), and 07.34.21.0011.01 [29], after some rigorous mathematics, the final closed-form expression of the ABER during jamming active is given by Appendix A (A1).

When the jamming is idle, according to [34], and assuming perfect Channel State Information at the receiver, the expression for BER is as follows:

$$P_{e1i-SIMO}(\overline{\gamma}_D) = \int_0^\infty \int_0^\infty \cdots \int_0^\infty f_{\gamma_{11}}(\gamma_{11}) f_{\gamma_{12}}(\gamma_{12}) \cdots f_{\gamma_{13}}(\gamma_{13})$$
$$\times Q\left(\frac{1}{2\sqrt{N}} \sqrt{\sum_{n=1}^{N} \gamma_{1n}} \right) d\gamma_{11} d\gamma_{12} \cdots d\gamma_{1N} \tag{41}$$

where, γ_{1n} represents the SNR from the transmitter to the nth receiver, while N denotes the total number of receivers. The Q-function can be approximated as $Q(x) \approx \frac{1}{12}e^{-x^2/2} + \frac{1}{4}e^{-2x^2/3}$, we can obtain

$$P_{e1i-SIMO}(\overline{\gamma}_D) \approx \frac{1}{12} \prod_{n=1}^{N} \int_0^\infty f_{h_{in}}(h_{in}) \exp\left(-\frac{\overline{\gamma}_D h_{in}^2}{4N} \right) dh_{in}$$
$$+ \frac{1}{4} \prod_{n=1}^{N} \int_0^\infty f_{h_{in}}(h_{in}) \exp\left(-\frac{\overline{\gamma}_D h_{in}^2}{3N} \right) dh_{in} \tag{42}$$
$$= \frac{1}{12} \prod_{n=1}^{N} \mathrm{F}_1 + \frac{1}{4} \prod_{n=1}^{N} \mathrm{F}_2$$

where

$$\mathrm{F}_1 = \frac{\xi_p^2}{\Gamma(\alpha_p)\Gamma(\beta_p)} \frac{\xi_q^2}{\Gamma(\alpha_q)\Gamma(\beta_q)} \frac{2^{(\alpha_p + \beta_p + \alpha_q + \beta_q - 7)}}{\sqrt{\pi}(\pi)^2}$$
$$\times G_{12,5}^{1,12} \left(\frac{64\overline{\gamma}_D}{N} \left(\frac{\alpha_p \beta_p \alpha_q \beta_q}{A_{0_p} A_{0_q}} \right)^{-2} \middle| \begin{array}{c} \mathbf{E}_1, \mathbf{E}_2, \mathbf{E}_3 \\ 0, \frac{-\xi_q^2}{2}, \frac{1-\xi_q^2}{2}, \frac{-\xi_p^2}{2}, \frac{1-\xi_p^2}{2} \end{array} \right) \tag{43}$$

$$\mathrm{F}_2 = \frac{\xi_p^2}{\Gamma(\alpha_p)\Gamma(\beta_p)} \frac{\xi_q^2}{\Gamma(\alpha_q)\Gamma(\beta_q)} \frac{2^{(\alpha_p + \beta_p + \alpha_q + \beta_q - 7)}}{\sqrt{\pi}(\pi)^2}$$
$$\times G_{12,5}^{1,12} \left(\frac{256\overline{\gamma}_D}{3N} \left(\frac{\alpha_p \beta_p \alpha_q \beta_q}{A_{0_p} A_{0_q}} \right)^{-2} \middle| \begin{array}{c} \mathbf{E}_1, \mathbf{E}_2, \mathbf{E}_3 \\ 0, \frac{-\xi_p^2}{2}, \frac{1-\xi_p^2}{2}, \frac{-\xi_q^2}{2}, \frac{1-\xi_q^2}{2} \end{array} \right) \tag{44}$$

where $\mathbf{E}_1 = \frac{1-\xi_p^2}{2}, \frac{2-\xi_p^2}{2}, \frac{1-\alpha_p}{2}, \frac{2-\alpha_p}{2}$, $\mathbf{E}_2 = \frac{1-\beta_p}{2}, \frac{2-\beta_p}{2}, \frac{1-\xi_q^2}{2}, \frac{2-\xi_q^2}{2}$, $\mathbf{E}_3 = \frac{1-\alpha_q}{2}, \frac{2-\alpha_q}{2}, \frac{1-\beta_q}{2}, \frac{2-\beta_q}{2}$.

Now, we can calculate the ABER for Scenario 1 of SIMO-FSO as follows

$$P_{e1-SMIO} = \rho P_{e1a-SIMO}\left(\overline{\gamma}_J \right) + (1 - \rho) P_{e1i-SIMO}(\gamma_D) \tag{45}$$

4.3.2. Analysis of the ABER for SIMO in Scenario 2

Since Scenario 2 has the same system model as Scenario 1 when jamming is idle, we only need to calculate the BER when jamming is active in Scenario 2.

Let $g_{Jsum} = \sum_{n=1}^{N} g_{Jn}$, then applying the Mellin transform to (11) with the transformation function 07.34.22.0004.01, we can obtain

$$
\begin{aligned}
\varphi_{h_{Jn}}(z) = {} & \left[1 - \exp\left(-\frac{\varphi_{AoA}^2}{2\sigma_{AoA}^2}\right)\right] \frac{\alpha_J \beta_J \xi_J^2}{A_{0_J} \Gamma(\alpha_J) \Gamma(\beta_J)} \\
& \times \left(\frac{\alpha_J \beta_J}{A_{0_J}}\right)^{-z} \frac{\Gamma(\xi_J^2 - 1 + z)\Gamma(\alpha_J - 1 + z)\Gamma(\beta_J - 1 + z)}{\Gamma(\xi_J^2 + z)}
\end{aligned}
\tag{46}
$$

Thus we have

$$
\varphi_{g_{Jsum}}(z) = \prod_{n=1}^{N} \varphi_{g_{Jn}}(z) = \left(\varphi_{g_{Jn}}(z)\right)^N
\tag{47}
$$

The Mellin inverse transform of (53) can be obtained as:

$$
\begin{aligned}
f_{g_{Jsum}}(x) = {} & \left(\frac{\alpha_q \beta_q \xi_q^2}{A_{0_q} \Gamma(\alpha_q) \Gamma(\beta_q)} \left[1 - \exp\left(-\frac{\varphi_{AoA}^2}{2\sigma_{AoA}^2}\right)\right] \frac{\alpha_J \beta_J \xi_J^2}{A_{0_J} \Gamma(\alpha_J) \Gamma(\beta_J)}\right)^N \\
& \times G_{2N,6N}^{6N,0}\left(\left(\frac{\alpha_J \beta_J \alpha_q \beta_q}{A_{0_J} A_{0_q}}\right)^N \times \left| \begin{matrix} \mathbf{C}_1 \\ \mathbf{C}_2, \mathbf{C}_3, \mathbf{C}_4 \end{matrix} \right.\right)
\end{aligned}
\tag{48}
$$

where $\mathbf{C}_1 = \overbrace{\xi_J^2, \cdots, \xi_J^2}^{N}, \overbrace{\xi_q^2, \cdots, \xi_q^2}^{N}$, $\mathbf{C}_2 = \underbrace{\xi_q^2 - 1, \cdots \xi_q^2 - 1}_{N}, \underbrace{\alpha_q - 1, \cdots, \alpha_q - 1}_{N}$,

$\mathbf{C}_3 = \underbrace{\beta_q - 1, \cdots, \beta_q - 1}_{N}, \underbrace{\xi_J^2 - 1, \cdots, \xi_J^2 - 1}_{N}$, and $\mathbf{C}_4 = \underbrace{\alpha_J - 1, \cdots, \alpha_J - 1}_{N}, \underbrace{\beta_J - 1, \cdots, \beta_J - 1}_{N}$.

From (48), we can obtain

$$
f_{y_{I-D}}(y_{I-D}) = \begin{cases}
\begin{aligned}
& \frac{1}{\sqrt{N_J}} \left(\frac{\alpha_q \beta_q \xi_q^2}{A_{0_q} \Gamma(\alpha_q) \Gamma(\beta_q)} \left[1 - \exp\left(-\frac{\varphi_{AoA}^2}{2\sigma_{AoA}^2}\right)\right] \frac{\alpha_J \beta_J \xi_J^2}{A_{0_J} \Gamma(\alpha_J) \Gamma(\beta_J)}\right)^N \\
& \times G_{2N,6N}^{6N,0}\left(\left(\frac{\alpha_J \beta_J \alpha_q \beta_q}{A_{0_J} A_{0_q}}\right)^N \frac{y_{I-D}}{\sqrt{N_J}} \left| \begin{matrix} \mathbf{C}_1 \\ \mathbf{C}_2, \mathbf{C}_3, \mathbf{C}_4 \end{matrix} \right.\right), & \text{for } s = 0
\end{aligned} \\
\begin{aligned}
& \frac{1}{\sqrt{N_J}} \left(\frac{\alpha_q \beta_q \xi_q^2}{A_{0_q} \Gamma(\alpha_q) \Gamma(\beta_q)} \left[1 - \exp\left(-\frac{\varphi_{AoA}^2}{2\sigma_{AoA}^2}\right)\right] \frac{\alpha_J \beta_J \xi_J^2}{A_{0_J} \Gamma(\alpha_J) \Gamma(\beta_J)}\right)^N \\
& \times G_{2N,6N}^{6N,0}\left(\left(\frac{\alpha_J \beta_J \alpha_q \beta_q}{A_{0_J} A_{0_q}}\right)^N \frac{y_{I-D} - \sqrt{P_s} \sum_{n=1}^{N} h_{in}}{\sqrt{N_J}} \left| \begin{matrix} \mathbf{C}_1 \\ \mathbf{C}_2, \mathbf{C}_3, \mathbf{C}_4 \end{matrix} \right.\right), & \text{for } s = 1
\end{aligned}
\end{cases}
\tag{49}
$$

From (18) and (49), and $h_{sum} = \sum_{n=1}^{N} a_n h_{in}$, we get:

$$
\begin{aligned}
P_{e2a-SIMO}(h_{isum}) = {} & \frac{\rho}{2} \sqrt{\rho \overline{\gamma}_{JD}} h_{isum} \left(\frac{\alpha_q \beta_q \xi_q^2}{A_{0_q} \Gamma(\alpha_q) \Gamma(\beta_q)} \left[1 - \exp\left(-\frac{\varphi_{AoA}^2}{2\sigma_{AoA}^2}\right)\right] \frac{\alpha_J \beta_J \xi_J^2}{A_{0_J} \Gamma(\alpha_J) \Gamma(\beta_J)}\right)^N \\
& \times G_{2N+1,6N+1}^{6N+1,0}\left(\left(\frac{\alpha_J \beta_J \alpha_q \beta_q}{A_{0_J} A_{0_q}}\right)^N \sqrt{\rho \overline{\gamma}_{JD}} h_{isum} \left| \begin{matrix} \mathbf{C}_1, 0 \\ -1, \mathbf{C}_2, \mathbf{C}_3, \mathbf{C}_4 \end{matrix} \right.\right)
\end{aligned}
\tag{50}
$$

By using (48) and (50), ABER can be obtained by Appendix A (A2).

Now, we can calculate the ABER for Scenario 2 of SIMO-FSO as follows:

$$
P_{e2-SMIO} = \rho P_{e2a-SIMO}\left(\overline{\gamma}_J\right) + (1 - \rho) P_{e1i-SIMO}(\gamma_D)
\tag{51}
$$

5. Numerical Results

Unless otherwise stated, $\xi_p = 1.2528$, $\varphi_{AoA} = 8$ mrad, $d_p = 1$ mm, $d_q = 3$ mm, and $\varphi_p = 0.175$ mrad. The following simulation results were obtained by using MATLAB 2022.

When $\xi_q = 1.2528$, $\xi_J = 1.2528$, $\alpha_p = 2.49$, $\beta_p = 3.9$, $\alpha_q = 4.0$, $\beta_q = 1.9$, $\alpha_J = 4.0$, $\beta_J = 1.9$, Figure 2 illustrates the variation of ABER with SJR obtained by (21), and Monte Carlo simulation at $\rho = 1$. It can be observed from Figure 2 that the concordance between the analytical and simulation plots validates the accuracy of the derived expression. It can be observed from Figure 2 that as the receiving aperture N increases, the ABER shows significant improvement. However, with the increase of SJR, the degree of improvement decreases. This is because the jamming signal only jams one of the receiving apertures, and under high SJR, each receiving aperture can effectively receive signals. Since the additive white Gaussian noise is not considered in Figure 2, when SJR is high, increasing the number of receiving apertures cannot significantly improve the ABER when the SJR is large. When N = 5, the improvement of ABER with SJR increasing is not very obvious. The reason is that increasing the number of receiving apertures can effectively suppress the influence of jamming. At the same time, even though the additive Gaussian white noise is not considered, the FSO system are also affected by path loss, PE, and AT, which are a static variable, so the changing trend of ABER with SJR is not obvious.
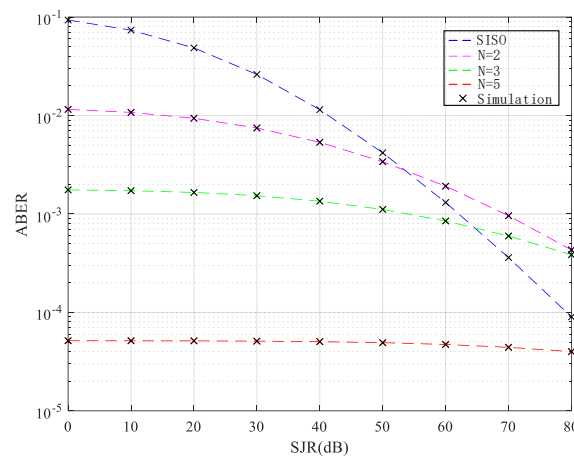

Figure 2. ABER versus SJR (dB) curves for an FSO system with a varying number of receiver apertures without considering additive Gaussian noise in Scenario 1.

Let $k = \frac{P_J}{N_0} = 100$. In scenario 1, the relationship between SJR and ABER is illustrated in Figure 3, which is derived from (26) and (45). Similarly, the relationship between SJR and ABER for scenario 2 is depicted in Figure 4, derived from (28) and (51). From Figures 3 and 4, it can be observed that for SISO-FSO systems, as the jamming probability ρ increases, the ABER also increases; For SIMO-FSO systems, when SJR is greater than 20dB, the ABER shows a positive correlation with ρ. Conversely, when SJR is less than 20dB, ABER decreases as ρ increases. This is because the use of SIMO technology enables effective signal recovery at high SJR. By comparing Figures 3 and 4, it is observed that jamming at the receiver has a significant impact on the system's BER at the RIS. For instance, when $\rho = 0.01$ and $\overline{\gamma}_J = 60$ dB, ABER for Scenario 1 with SISO and SIMO are 3.49×10^{-4} and 4.77×10^{-5}, respectively. For Scenario 2, ABER with SISO and SIMO are 9.08×10^{-5} and 1.35×10^{-6}, respectively. This indicates that jamming at the receiver has a greater impact on the system compared to interference at the RIS.

In Figure 5, we analyze the impact of different atmospheric turbulence on the ABER in two scenarios. The analytical plots closely align with the Monte Carlo simulations conducted, thereby confirming the accuracy of the derived expressions. It can be observed from Figure 5 that the system's overall performance improves as the turbulence ranges from strong ($\alpha_p = 4.0$, $\beta_p = 1.9$) to moderate ($\alpha_p = 2.49$, $\beta_p = 3.9$). Nevertheless, under the same turbulence parameters, the ABER performance for Scenario 1 is notably inferior to that of Scenario 2. This suggests that jamming at the RIS has a smaller impact on the system compared to jamming at the intended receiver of the legitimate signal. One possible reason for this is that the RIS distributes the power of the jamming signal.
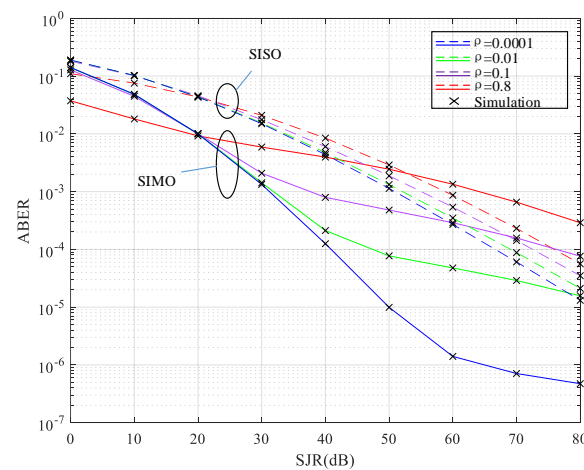
Figure 3. ABER versus SJR (dB) curves for an FSO system with a varying ρ with considering additive Gaussian noise in Scenario 1.
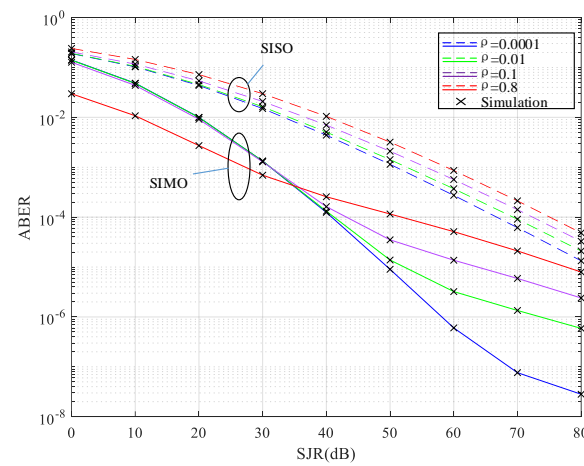

Figure 4. ABER versus SJR (dB) curves for an FSO system with a varying ρ with considering additive Gaussian noise in Scenario 2.
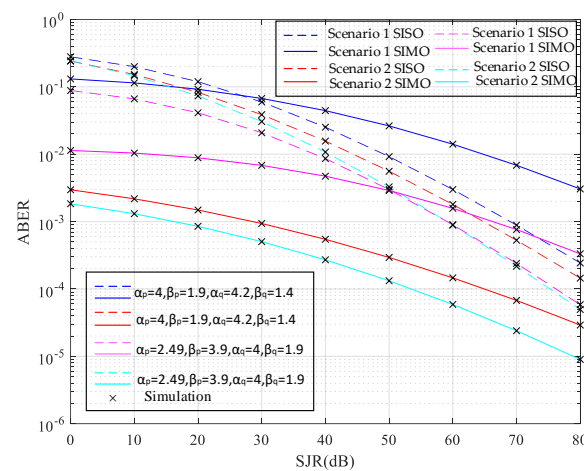

Figure 5. Comparison of ABER between the two scenarios under varying turbulence parameters.

Figures 6 and 7 analyze the impact of the RIS location on the system ABER in two scenarios. Let $\eta = L_p/L_q$, where L_p is the link length between S and RIS and L_q is the link length between RIS and the destination [19]. Based on the value of η, the value of ξ_q^2 can be calculated according to [20], with other simulation parameters set to $\xi_p = 4.5856$,

$\alpha_p = \alpha_q = 5.4$, $\beta_p = \beta_q = 3.77$, and $\rho = 0.5$. As η decreases, it indicates that the RIS is relatively closer to the source node than the destination node. From Figures 6 and 7, it can be observed that a smaller value of η leads to better system ABER performance. Therefore, it should be positioned as close to the source node as possible. Furthermore, it is noted that under weak turbulence with jamming present, the adoption of SIMO technology does not effectively enhance the ABER in Scenario 1, as depicted in Figure 6. However, in Scenario 2, SIMO notably improves the ABER, as shown in Figure 7. This phenomenon is attributed to the minimal channel attenuation in weak turbulence conditions, where the introduction of multiple additive Gaussian noises in SIMO results in an increase in the ABER. Therefore, it is not recommended to employ SIMO technology to mitigate jamming in Scenario 1 under weak turbulence conditions.
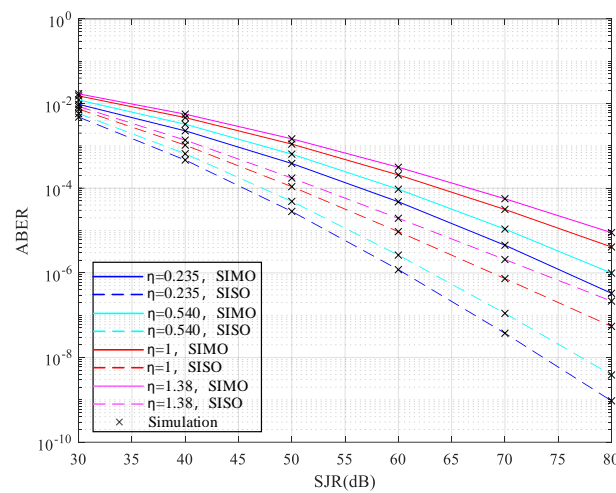

Figure 6. Analysis of ABER for different RIS positions in Scenario 1.
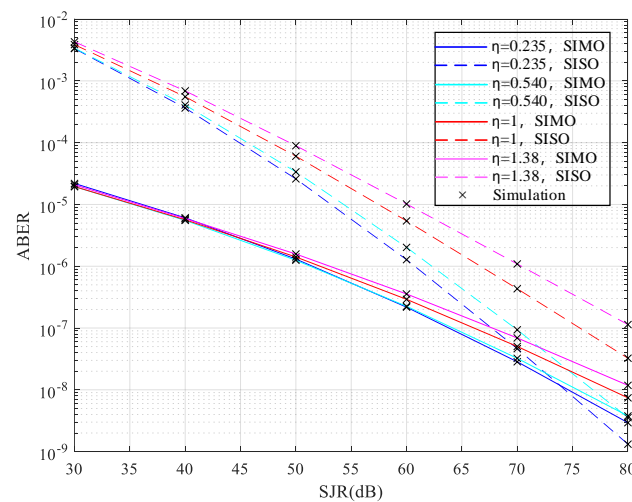

Figure 7. Analysis of ABER for different RIS positions in Scenario 2.

Computational complexity analysis: From (45), and (51), it can be concluded that the computational complexity of ABER using SIMO is $O(N^3)$. When N is large, the computational complexity of (45), and (51) is high. When N is small, the complexity is relatively small. Since SIMO is typically employed in FSO with 2 receiving apertures [24], our proposed ABER calculation can be effectively applied to FSO systems.

6. Conclusions

We have conducted a study on the impact of jamming in an RIS-assisted Dual-Hop FSO Communication system in the presence of a malicious jammer. A novel PDF for the S-IRS-D, UAV-IRS-D, and UAV-D links under the combined influence of AT, PE, and AoA fluctuations has been developed. Based on the jamming scenario, closed-form expressions for the end-to-end ABER have been derived for SISO-FSO systems. To mitigate the impact of jamming in an RIS-assisted Dual-Hop FSO Communication system, a SIMO FSO system has been implemented. We have utilized the Mellin transform to derive the PDF of the legitimate channel and the jamming channel in the SIMO FSO system and the end-to-end ABER have been derived for SIMO-FSO systems under different jamming Scenarios. The simulation results are compared with the analytical results to validate the accuracy of the derived expression. It has been observed that as the number of receiving apertures increases, the system shows a significant improvement in bit error performance. For the SISO and 1×2 FSO systems, we conducted separate analyses on the impact of different jamming probabilities. In Scenario 1, the jamming occurs at D, while in Scenario 2, the jamming occurs at the RIS, affecting the system's ABER. In regions with low SJR regions, it was found that ABER is inversely proportional to the jamming probability ρ; conversely, in relatively high SJR regions, ABER exhibits a direct proportionality with ρ. Simultaneously, the jamming in Scenario 1 has a greater impact on the system's ABER compared to the interference in Scenario 2. The impact of different positions of the RIS on the overall system performance has also been investigated. The system achieves optimal performance when the RIS is situated in closer proximity to the source.

Author Contributions: Conceptualization, J.W. and D.G.; methodology, J.W.; software, J.L.; validation, J.W., L.H. and H.D.; formal analysis, S.Z.; investigation, J.W.; resources, D.G.; data curation, J.L.; writing—original draft preparation, J.W.; writing—review and editing, H.D.; visualization, J.W.; supervision, D.G.; project administration, D.G.; funding acquisition, H.D. All authors have read and agreed to the published version of the manuscript.

Data Availability Statement: Data will be made available on request.

Conflicts of Interest: The authors declare no conflict of interest.

Appendix A

$$
P_{e1a-SIMO}\left(\overline{\gamma}_J\right) = \left(\frac{A_{0p}A_{0q}\xi_p^2}{\alpha_p\beta_p\alpha_q\beta_q\Gamma(\alpha_p)\Gamma(\beta_p)}\frac{\xi_q^2}{\Gamma(\alpha_q)\Gamma(\beta_q)}\right)^N \frac{\rho}{2}\left[1-\exp\left(-\frac{\varphi_{AoA}^2}{2\sigma_{AoA}^2}\right)\right]
$$
$$
\times \frac{\alpha_J\beta_J\xi_J^2\sqrt{\rho\overline{\gamma}_J}}{A_{0J}\Gamma(\alpha_J)\Gamma(\beta_J)}G_{6N+2,2N+4}^{4,6N}\left(\frac{\alpha_J\beta_J\sqrt{\rho\overline{\gamma}_J}}{A_{0J}}\left(\frac{\alpha_p\beta_p\alpha_q\beta_q}{A_{0p}A_{0q}}\right)^{-N}\middle|\begin{array}{c} \mathbf{Z}_1,\mathbf{Z}_2,\mathbf{Z}_3,\xi_J^2,0 \\ -1,\xi_J^2-1,\alpha_J-1,\beta_J-1,\mathbf{Z}_4 \end{array}\right) \quad (A1)
$$

where $\mathbf{Z}_1 = \underbrace{-\xi_p^2,\cdots,-\xi_p^2}_{N},\underbrace{-\alpha_p,\cdots,-\alpha_p}_{N}$, $\mathbf{Z}_2 = \underbrace{-\beta_p,\cdots,-\beta_p}_{N},\underbrace{-\xi_q^2,\cdots,-\xi_q^2}_{N}$,

$\mathbf{Z}_3 = \underbrace{-\alpha_q,\cdots,-\alpha_q}_{N},\underbrace{-\beta_q,\cdots,-\beta_q}_{N}$, and $\mathbf{Z}_4 = \overbrace{-1-\xi_p^2,\cdots,-1-\xi_p^2}^{N},\overbrace{-1-\xi_q^2,\cdots,-1-\xi_q^2}^{N}$.

$$
P_{e2a-SIMO}\left(\overline{\gamma}_{JD}\right) = \left(\frac{\xi_q^2}{\Gamma(\alpha_q)\Gamma(\beta_q)}\left[1-\exp\left(-\frac{\varphi_{AoA}^2}{2\sigma_{AoA}^2}\right)\right]\frac{\alpha_J\beta_J\xi_J^2}{A_{0J}\Gamma(\alpha_J)\Gamma(\beta_J)}\right)^N
$$
$$
\times \left(\frac{\xi_p^2}{\Gamma(\alpha_p)\Gamma(\beta_p)}\frac{\xi_q^2}{\Gamma(\alpha_q)\Gamma(\beta_q)}\right)^N \frac{\rho}{2}\sqrt{\rho\overline{\gamma}_{JD}}\left(\frac{A_{0p}}{\alpha_p\beta_p}\right)^{2N} \quad (A2)
$$
$$
\times G_{8N+1,8N+1}^{6N+1,6N}\left(\left(\frac{\alpha_J\beta_J A_{0p}}{\alpha_p\beta_p A_{0J}}\right)^N \sqrt{\rho\overline{\gamma}_{JD}}\middle|\begin{array}{c} X_1,X_2,X_3 \\ X_4,X_5,X_6 \end{array}\right)
$$

$$\text{where} \quad X_1 \;=\; \overbrace{-\xi_p^2, \cdots, -\xi_p^2}^{N}, \overbrace{-\alpha_p, \cdots, -\alpha_p}^{N}, \overbrace{-\beta_p, \cdots, -\beta_p}^{N}, \quad X_2 \;=\; \overbrace{-\xi_q^2, \cdots, -\xi_q^2}^{N},$$

$$\overbrace{-\alpha_q, \cdots, -\alpha_q}^{N}, \overbrace{-\beta_q, \cdots, -\beta_q}^{N}, X_3 = \overbrace{\xi_q^2, \cdots, \xi_q^2}^{N}, \overbrace{\xi_J^2, \cdots, -\xi_J^2}^{N}, 0, X_4 = -1, \overbrace{\xi_q^2 - 1, \cdots, \xi_q^2 - 1}^{N},$$

$$\overbrace{\alpha_q - 1, \cdots, \alpha_q - 1}^{N}, \quad X_5 \;=\; \overbrace{\beta_q - 1, \cdots, \beta_q - 1}^{N}, \overbrace{\xi_J^2 - 1, \cdots, \xi_J^2 - 1}^{N}, \overbrace{\alpha_J - 1, \cdots, \alpha_J - 1}^{N}, \quad \text{and}$$

$$X_6 = \overbrace{\beta_J - 1, \cdots, \beta_J - 1}^{N}, \overbrace{-1 - \xi_p^2, \cdots, -1 - \xi_p^2}^{N}, \overbrace{-1 - \xi_q^2, \cdots, -1 - \xi_q^2}^{N}.$$

References

1. Mishra, P.; Singh, G. Energy management systems in sustainable smart cities based on the internet of energy: A technical review. *Energies* **2023**, *16*, 6903. [CrossRef]
2. Huang, Y.; Jin, J.; Lou, M.; Dong, J.; Wu, D.; Xia, L.; Wang, S.; Zhang, X. 6G mobile network requirements and technical feasibility study. *China Commun.* **2022**, *19*, 123–136. [CrossRef]
3. Wang, J.; Li, J.; Chen, D.; Dong, Y.; Ding, H.; Gao, D. Performance analysis and verification of FSO based inter-ship communication systems on sea. *Opt. Commun.* **2024**, *557*, 130271. [CrossRef]
4. Elamassie, M.; Uysal, M. Free space optical communication: An enabling backhaul technology for 6G non-terrestrial networks. *Photonics* **2023**, *10*, 1210. [CrossRef]
5. Raj, A.A.B.; Krishnan, P.; Darusalam, U.; Kaddoum, G.; Ghassemlooy, Z.; Abadi, M.M.; Majumdar, A.K.; Ijaz, M. A review–unguided optical communications: Developments, technology evolution, and challenges. *Electronics* **2023**, *12*, 1922. [CrossRef]
6. Yücel, M.; Açikgöz, M. Optical communication infrastructure in new generation mobile networks. *Fiber Integr. Opt.* **2023**, *42*, 53–92. [CrossRef]
7. Hayal, M.R.; Yousif, B.B.; Azim, M.A. Performance enhancement of DWDM-FSO optical fiber communication systems based on hybrid modulation techniques under atmospheric turbulence channel. *Photonics* **2021**, *8*, 464. [CrossRef]
8. Al-Nahhal, M.; Ismail, T. Enhancing spectral efficiency of FSO system using adaptive SIM/M-PSK and SIMO in the presence of atmospheric turbulence and pointing errors. *Int. J. Commun. Syst.* **2019**, *32*, e3942. [CrossRef]
9. Ismail, T.; Leitgeb, E.; Ghassemlooy, Z.; Al-Nahhal, M. Performance improvement of FSO system using multi-pulse pulse position modulation and SIMO under atmospheric turbulence conditions and with pointing errors. *IET Netw.* **2018**, *7*, 165–172. [CrossRef]
10. Xu, M.; Xu, G.; Dong, Y.; Wang, W.; Zhang, Q.; Song, Z. UAV-assisted FSO communication system with amplify-and-forward protocol under AOA fluctuations: A performance analysis. *China Commun.* **2023**, *20*, 111–130. [CrossRef]
11. Chapala, V.K.; Zafaruddin, S.M. Unified performance analysis of reconfigurable intelligent surface empowered free-space optical communications. *IEEE Trans. Commun.* **2021**, *70*, 2575–2592. [CrossRef]
12. Najafi, M.; Schmauss, B.; Schober, R. Intelligent reflecting surfaces for free space optical communication systems. *IEEE Trans. Commun.* **2021**, *69*, 6134–6151. [CrossRef]
13. Basar, E.; Poor, H.V. Present and future of reconfigurable intelligent surface-empowered communications [perspectives]. *IEEE Signal Process. Mag.* **2021**, *38*, 146–152. [CrossRef]
14. Aboagye, S.; Ndjiongue, A.R.; Ngatched, T.M.; Dobre, O.A.; Poor, H.V. RIS-assisted visible light communication systems: A tutorial. *IEEE Commun. Surv. Tutor.* **2022**, *25*, 251–288. [CrossRef]
15. Basar, E.; Di Renzo, M.; De Rosny, J.; Debbah, M.; Alouini, M.-S.; Zhang, R. Wireless communications through reconfigurable intelligent surfaces. *IEEE Access* **2019**, *7*, 116753–116773. [CrossRef]
16. Ali, M.F.; Jayakody, D.N.K.; Garg, S.; Kaddoum, G.; Hossain, M.S. Dual-hop mixed FSO-VLC underwater wireless communication link. *IEEE Trans. Netw. Serv. Manag.* **2022**, *19*, 3105–3120. [CrossRef]
17. Zhang, S.; Zhu, D.; Liu, Y. Artificial intelligence empowered physical layer security for 6G: State-of-the-art, challenges, and opportunities. *Comput. Netw.* **2024**, *242*, 110255. [CrossRef]
18. Ndjiongue, A.R.; Ngatched, T.M.; Dobre, O.A.; Armada, A.G.; Haas, H. Analysis of RIS-based terrestrial-FSO link over GG turbulence with distance and jitter ratios. *J. Light. Technol.* **2021**, *39*, 6746–6758. [CrossRef]
19. Huang, J.; Wang, C.-X.; Sun, Y.; Feng, R.; Huang, J.; Guo, B.; Zhong, Z.; Cui, T.J. Reconfigurable intelligent surfaces: Channel characterization and modeling. *Proc. IEEE* **2022**, *110*, 1290–1311. [CrossRef]
20. Li, X.; Li, Y.; Song, X.; Shao, L.; Li, H. RIS assisted UAV for weather-dependent satellite terrestrial integrated network with hybrid FSO/RF systems. *IEEE Photonics J.* **2023**, *15*, 7304217. [CrossRef]
21. Paul, P.; Bhatnagar, M.R. Jamming Threats in Free-Space Optics. *IEEE Commun. Mag.* **2022**, *60*, 104–108. [CrossRef]
22. Jahid, A.; Alsharif, M.H.; Hall, T.J. A contemporary survey on free space optical communication: Potentials, technical challenges, recent advances and research direction. *J. Netw. Comput. Appl.* **2022**, *200*, 103311. [CrossRef]
23. Dong, Y.; Sadegh Aminian, M. Routing in Terrestrial Free Space Optical Ad-Hoc Networks. Master's Thesis, Linköping University Electronic Press: Linköping, Sweden, 21 November 2014.
24. Paul, P.; Bhatnagar, M.R.; Jaiswal, A. Alleviation of jamming in free space optical communication over Gamma-Gamma channel with pointing errors. *IEEE Photonics J.* **2019**, *11*, 7906418. [CrossRef]

25. Paul, P.; Bhatnagar, M.R.; Nebhen, J. Pulse jamming in aperture-averaged fso receiver over exponentiated weibull fading channel. *IEEE Trans. Wirel. Commun.* **2021**, *21*, 4242–4254. [CrossRef]
26. Shukla, A.K.; Bhatnagar, M.R. Mitigating Jamming in FSO Cooperative Networks: A Buffer-Aided Relaying Approach. *IEEE Commun. Lett.* **2023**, *27*, 2078–2082. [CrossRef]
27. Saxena, P.; Chung, Y.H. Analysis of jamming effects in IRS assisted UAV dual-hop FSO communication systems. *IEEE Trans. Veh. Technol.* **2023**, *72*, 8956–8971. [CrossRef]
28. Chauhan, I.; Bhatnagar, M.R. UAV-Based FSO Communication Under Jamming. In Proceedings of the 2022 IEEE 95th Vehicular Technology Conference:(VTC2022-Spring), Helsinki, Finland, 19–22 June 2022; pp. 1–5.
29. Wolfram Research. Available online: http://functions.wolfram.com/06.27.21.0133.01 (accessed on 27 April 2018).
30. Dabiri, M.T.; Sadough, S.M.S.; Khalighi, M.A. Channel modeling and parameter optimization for hovering UAV-based free-space optical links. *IEEE J. Sel. Areas Commun.* **2018**, *36*, 2104–2113. [CrossRef]
31. Saxena, P.; Bhatnagar, M.R. A simplified form of beam spread function in underwater wireless optical communication and its applications. *IEEE Access* **2019**, *7*, 105298–105313. [CrossRef]
32. Roach, K. Meijer G function representations. In Proceedings of the 1997 International Symposium On symbolic and Algebraic Computation, Kihei, HI, USA, 21–23 July 1997.
33. Pang, W.; Wang, P.; Li, S.; Li, H.; Song, X. Reliability analysis of optical IRS-enabled FSO system with multiple detectors and PCB under composite turbulence fading channels considering the impact of GML. *Opt. Commun.* **2023**, *537*, 129465. [CrossRef]
34. Tsiftsis, T.A.; Sandalidis, H.G.; Karagiannidis, G.K.; Uysal, M. Optical wireless links with spatial diversity over strong atmospheric turbulence channels. *IEEE Trans. Wirel. Commun.* **2009**, *8*, 951–957. [CrossRef]